InSAR phase estimation advances for high-resolution TanDEM-X DEM generation

Francescopaolo Sica, Nicola Gollin, Giorgia Gobbi, and Paola Rizzoli
Microwave and radar institute, German Aerospace Center (DLR), Oberpfaffenhofen, Germany

Abstract

Synthetic Aperture Radar Interferometry (InSAR) is nowadays a well established technique for the retrieval of ground topography from radar space-borne sensors. The TanDEM-X mission has provided high-resolution data at the X-band in a bistatic configuration, allowing for the generation of Digital Elevation Model (DEM) products with an unprecedented level of accuracy and resolution. The DEM quality is strongly influenced by the processing technique that is used for the retrieval of the interferometric phase from noisy SAR acquisitions. For this reason, the development of advanced processing techniques able to preserve DEM's resolution and accuracy is a critical step for the whole interferometric processing chain. In this work, we present the last advances for the retrieval of the interferometric phase and assess the performance on the generated DEM.

1 Introduction

Space-borne sensors are nowadays largely used for the generation of surface topography. Synthetic Aperture Radar Interferometry (InSAR) exploits a pair of SAR images acquired from slighlty different point of view to retrieve a Digital Elevation Model (DEM) of the illuminated scene. The accuracy of the height measurement depends from the sensor's operational bandwidht as well as the acquisition geometry of the interferometric system. This methodology has been successfully applied in the SRTM (Shuttle Radar Topography Measurement) and the latest TanDEM-X missions started in 2000 and 2010, respectively. These missions have provided DEMs at a nearly global scale by exploiting bistatic interferometric acquisitions. The TanDEM-X mission consists of two twin satellites flying in a close orbit formation and providing interferometric acquisitions at X band. This mission has generated DEMs with a higher resolution and accuracy with respect to the SRTM mission. In particular, the maximal achieved horizontal resolution is 12x12 meters and relative vertical accuracy is 2 meters (4 meters) for terrains with a slope smaller (larger) than 20% [1].

SAR Interferometry relies on the phase difference between the two SAR acquisitions, normally named as interferometric phase. The information about the elevation is indeed encoded in the spatial variation of interferometric phase. In particular, the link between these two factors, phase variation $\Delta\phi$ and elevation Δz is given by the following relationship

$$\Delta\phi = 2\pi\frac{\Delta z}{h_{\text{amb}}}, \tag{1}$$

with h_{amb} the height of ambiguity, which expresses the elevation change, in meters, related to one interferometric fringe, i.e. 2π jump. For a bistatic system, this quantity is given by

$$h_{\text{amb}} = \frac{\lambda R\sin(\theta_i)}{B_\perp}, \tag{2}$$

where λ is the wavelength, R the range distance, and θ_i the incidence angle.

A lower height of ambiguity reduces the phase-to-height error scaling and hence, theoretically, it increases the accuracy of the elevation measurement, namely the vertical resolution. Likewise, it contributes to degrade the interferometric phase estimate due to the increased signal non-stationarity and to baseline-induced coherence losses.

Phase estimation techniques have direct impact on the final DEM quality and resolution. Patch-based filters, can adapt to local features and strongly reduce the noise power while preserving the fringes' structure [2, 3]. For this reason, such patch-based methods allow to achieve a resolution improvement in both spatial and vertical dimensions. Nonetheless, severe performance decay is observed for patch-based filters in presence of slopes which are normally characterized by a constant phase gradient. The reason is ascribed to the lack of a sufficient number of similar patches, which is typical of patch-based approaches. In [4] this issue is solved by modifying the similarity measure in order to consider patches with the same topography, rather than the same phase value. Following this concept, the set of candidate pixels is enlarged by considering also all those patches that differ from the target only for a constant phase value. This approach has been indicated as offset-compensated nonlocal filtering.

In this paper we analyze the performance on DEM accuracy of different state-of-the-art filters, with specific mention to patch based approaches. We exploit a test area over the austrian Alps, where a 10×10 meters LiDAR DEM is available. We compare the reconstruction of DEM profiles with respect to the LiDAR reference [5].

This paper is structured as follows: in Section 2 we provide an overview of the compared approaches and the concept of offset-compensation for patch-based approaches. Materials and methods for performance assessment are presented in Section 3 and the experimental results and conclusion are given in Sections 4 and 5, respectively.

2 Patch-based algorithms for InSAR phase estimation

Patch-based approaches exploit image self-similarities in order to compute the average over a dedicated set of pixels. These are selected from a neighborhood of the target pixel according to a given similarity criterion [6]. In the following, we indicate with z the SAR Single Look Complex (SLC) and with Γ the complex interferogram

$$z = Ae^{j\phi} \tag{3}$$

$$\Gamma = z_m \odot z_s^* = A_m A_s e^{j\theta} \tag{4}$$

where A and ϕ are the amplitude and the phase of the SLC, $\theta = \phi_m - \phi_s$ is the interferometric phase, the indexes m and s stand for master and slave SLCs, $*$ and $\odot$ are the conjugate operator and the Hadamard product respectively.
The nonlocal-means [6] applied to interferometric SAR data is given by

$$\hat{\Gamma}(p) = \sum_{q \in \Omega} w(p,q)\Gamma(q) \tag{5}$$

where p indicates the current pixel to be estimated and q represents the comparison pixel taken from a set of similar pixels Ω.
The weigths $w(p,q)$ express the similarity between interferometric patches, i.e. the image crop surrounding the considered pixel p. They are related, normally through an exponential kernel, to a dissimilarity measure D that computes the degree of similarity between current and comparison patches

$$w(p,q) = c \cdot \exp\{-\delta D(p,q)\} \tag{6}$$

being c a multiplicative constant and δ a parameter that trades off the smoothing with the detail preservation. The weight kernel in (6) is adapted depending on the local phase structure, while the filtering is performed as in (5). The used dissimilarity measure D_{NLS} is choosen accordingly to the type of data, indeed in [2] the authors derive its expression as a function of the generalized likelihood ratio between two interferometric patches (L_G)

$$D_{NLS}(p,q) = -\sum_{i \in patch} \log \frac{1}{L_G(p,q)} \tag{7}$$

The InSAR-BM3D [3] combines the patch-based pixel similarity with the Wiener filtering in the wavelet domain. The algorithm has two consecutive steps: the first one provides a pre-estimate to perform, at the second step, the actual filtering. For a given target pixel, the algorithm forms a group of similar patches in order to obtain a sparse representation of the signal in the wavelet domain and to apply a hard-thresholding and a Wiener filtering at the first and second step respectively. A suitable transform is applied to the input data before the filtering, in order to decorrelate and to process independently the real and imaginary part of the interferogram.
The dissimilarity measure D_{BM} is evaluated by means of the cosine distance on interferometric phase values θ

$$D_{BM}[\theta(p),\theta(q)] = 1 - \frac{1}{N}\sum_{i \in patch} \cos(\theta(p)_i - \theta(q)_i) \tag{8}$$

This distance correspond to the one used at the first step D_{BM1}, while at the second step, since a pre-estimate of the signal is available, D_{BM2} is a combination of the same measure on noisy θ and estimate $\hat{\theta}$ data

$$D_{BM1}(p,q) = D_{BM}[\theta(p),\theta(q)] \tag{9}$$

$$D_{BM2}(p,q) = \gamma D_{BM}(\hat{\theta}(p),\hat{\theta}(q)) + (1-\gamma) D_{BM}(\theta(p),\theta(q)) \tag{10}$$

where $\gamma liesintheinterval\,[0,1]$ and is set empirically.
Similarly, the offset compensated version is given as in [4] by

$$D_{OC}(p,q) = 1 - |\sum_{i \in patch} \frac{1}{N} e^{j(\theta(p)_i - \theta(q)_i)}|, \tag{11}$$

where the offset is expressed as

$$\psi(p,q) = \angle \sum_{i \in patch} e^{j(\theta(p)_i - \theta(q)_i)}. \tag{12}$$

This distance corresponds to the one used at the first step D_{OC1}, while at the second step, since a pre-estimate of the signal is available, D_{OC2} is a combination of the same measure on noisy θ and estimated $\hat{\theta}$ data

$$D_{OC1}(p,q) = D_{OC}[\theta(p),\theta(q)] \tag{13}$$

$$D_{OC2}(p,q) = \gamma D_{OC}(\hat{\theta}(p),\hat{\theta}(q)) + (1-\gamma) D_{OC}(\theta(p),\theta(q)) \tag{14}$$

3 Materials and methods

In the present work, we perform a complementary analysis to integrate the results provided in [4]. By exploiting the TAXI interferometric processor [7], we vary only the interferometric phase estimation algorithm (NLSAR, InSAR-BM3D, OC-InSAR-BM3D), while retaining the usual interferometric processing and then assess the quality of phase filtering directly on the generated DEMs.
Fig. 1 show the LiDAR DEM [5] corresponding to the selected test area over the Austrian Alps (Salzburg city). We selected a TanDEM-X interferometric pair, which has been acquired on the 24th August 2014 in ascending orbit and has a height of ambiguity of about 80 meters.

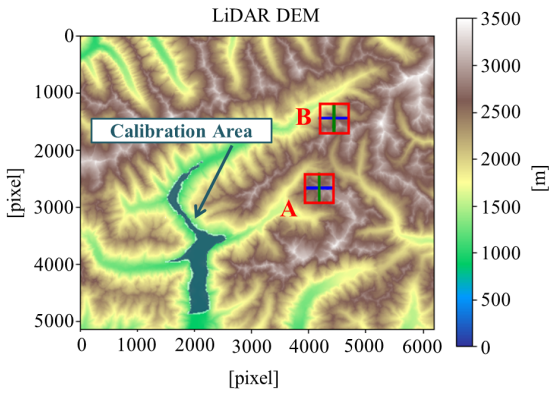

Figure 1 LiDAR DEM related to the test area (Austria). The red boxes indicate the cut chosen for the performance assessment.

4 Results

In order to assess the filter performance, we generate DEMs at 12 meters resolution by exploiting the TAXI interferometric processor [7]. We analyze the displacements between the generated DEMs and the LiDAR DEM, and in Fig. 2 we show some DEM lines for each of the compared algorithms.

In agreement with the comparison performed in [4], the OC-InSAR-BM3D performs better than each of the compared methods.

As expected, for large topography variation the OC-InSAR-BM3D provides the highest agreement with the LiDAR DEM, while for smoother areas the InSAR-BM3D provides the best match (Fig. 2). This result suggests to inhibit the offset compensation for areas with low topography variation as found in [4].

The NLSAR algorithm shows a DEM reconstruction very similar to the two BM3D-based methods but with slightly worse performance.

It is worth pointing out that the generation of DEMs from InSAR data in critical areas, such as mountainous regions, can benefit from the combination of several InSAR data acquired with different geometries in order to cope with the presence of geometric distortions due to layover and shadow.

5 Conclusions

The presented work has assessed the performance of latest patch-based filters for the generation of high-resolution Digital Elevation Model from TanDEM-X data. By retaining the same interferometric processing chain, only the phase estimation method is varied. The performance are computed on the final DEM product by extracting some sample transects along the longitude and latitude directions. The performance comparison confirms the analysis performed on interferometric phase estimation in [4]. The OC-InSAR-BM3D, in presence of dense fringe patterns provides the best DEM reconstruction. Indeed, only by exploiting the offset compensation within patch-based approaches, it is possible to retrieve correctly the elevation of mountain peaks. Future work will focus on the performance assessment varying the acquisition parameters, such as the height of ambiguity.

6 Literature

[1] Paola Rizzoli, Benjamin Bräutigam, Thomas Kraus, Michele Martone, and Gerhard Krieger, "Relative height error analysis of TanDEM-X elevation data," *ISPRS Journal of Photogrammetry and Remote Sensing*, vol. 73, pp. 30–38, 2012.

[2] Charles-Alban Deledalle, Loïc Denis, Florence Tupin, Andreas Reigber, and Marc Jäger, "NL-SAR: A unified nonlocal framework for resolution-preserving (Pol)(In) SAR denoising," *IEEE Transactions on Geoscience and Remote Sensing*, vol. 53, no. 4, pp. 2021–2038, 2015.

[3] Francescopaolo Sica, Davide Cozzolino, Xiao Xiang Zhu, Luisa Verdoliva, and Giovanni Poggi, "InSAR-BM3D: A nonlocal filter for SAR interferometric phase restoration," in *IEEE Transactions on Geoscience and Remote Sensing*, 2018.

[4] Francescopaolo Sica, Davide Cozzolino, Luisa Verdoliva, and Giovanni Poggi, "The offset-compensated nonlocal filtering of interferometric phase," *Remote Sensing*, vol. 10, no. 9, pp. 1359, 2018.

[5] "Digital terrain models of austria," http://data.opendataportal.at/dataset/dtm-austria.

[6] Antoni Buades, Bartomeu Coll, and J-M Morel, "A non-local algorithm for image denoising," in *Computer Vision and Pattern Recognition, 2005. CVPR 2005. IEEE Computer Society Conference on*. IEEE, 2005, vol. 2, pp. 60–65.

[7] Pau Prats, Marc Rodriguez-Cassola, Luca Marotti, Matteo Naninni, Steffen Wollstadt, Daniel Schulze, Núria Tous-Ramon, Marwan Younis, Gerhard Krieger, and Andreas Reigber, "Taxi: A versatile processing chain for experimental TanDEM-X product evaluation," in *Geoscience and Remote Sensing Symposium (IGARSS), 2010 IEEE International*. IEEE, 2010, pp. 4059–4062.

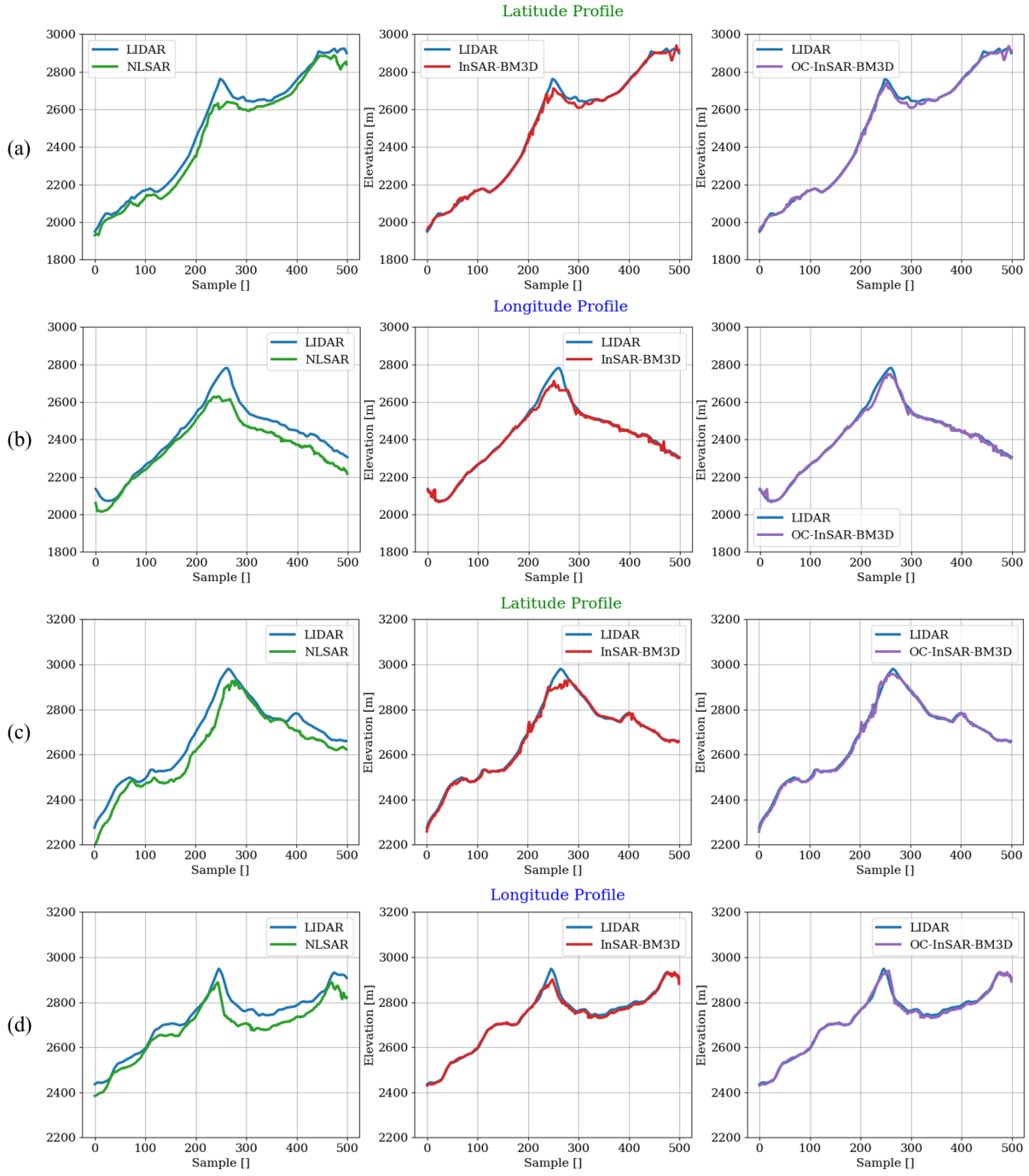

Figure 2 DEM line selected from the selected cut (red box in Fig.1). Each of the considered algorithms is compared with the reference LiDAR DEM.